Provided for non-commercial research and education use.
Not for reproduction, distribution or commercial use.

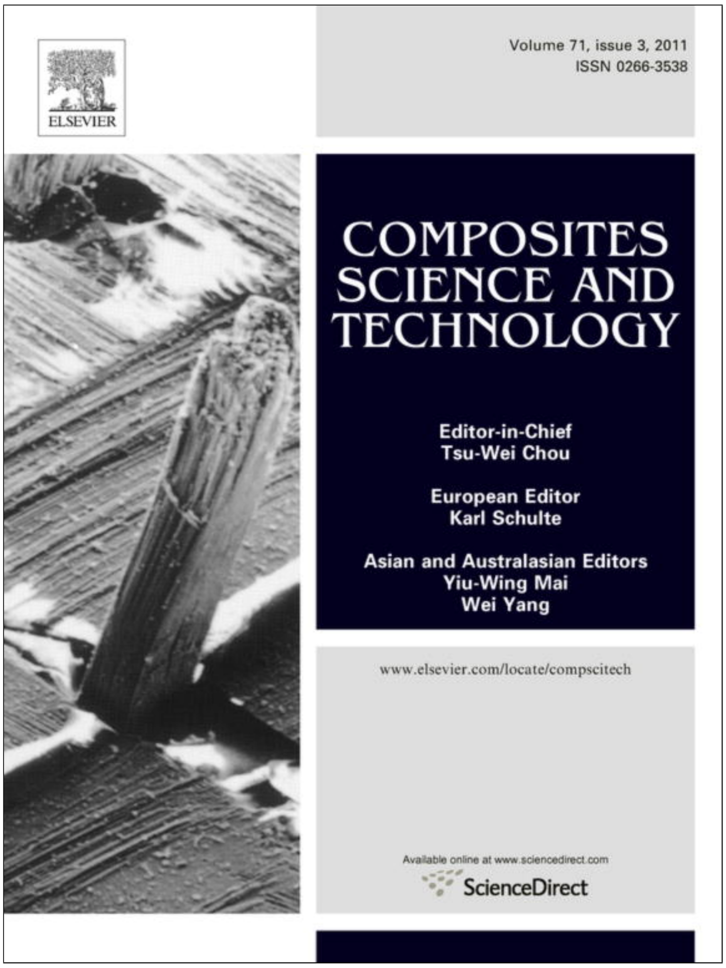

Volume 71, issue 3, 2011
ISSN 0266-3538

COMPOSITES SCIENCE AND TECHNOLOGY

Editor-in-Chief
Tsu-Wei Chou

European Editor
Karl Schulte

Asian and Australasian Editors
Yiu-Wing Mai
Wei Yang

www.elsevier.com/locate/compscitech

Available online at www.sciencedirect.com
ScienceDirect

This article appeared in a journal published by Elsevier. The attached copy is furnished to the author for internal non-commercial research and education use, including for instruction at the authors institution and sharing with colleagues.

Other uses, including reproduction and distribution, or selling or licensing copies, or posting to personal, institutional or third party websites are prohibited.

In most cases authors are permitted to post their version of the article (e.g. in Word or Tex form) to their personal website or institutional repository. Authors requiring further information regarding Elsevier's archiving and manuscript policies are encouraged to visit:

http://www.elsevier.com/copyright

Composites Science and Technology 71 (2011) 365–372

Contents lists available at ScienceDirect

Composites Science and Technology

journal homepage: www.elsevier.com/locate/compscitech

Failure mechanics of organic–inorganic multilayer permeation barriers in flexible electronics

Zheng Jia [a], Matthew B. Tucker [a], Teng Li [a,b,*]

[a] Department of Mechanical Engineering, University of Maryland, College Park, MD 20742, United States
[b] Maryland NanoCenter, University of Maryland, College Park, MD 20742, United States

ARTICLE INFO

Article history:
Received 22 May 2010
Received in revised form 21 November 2010
Accepted 1 December 2010
Available online 5 December 2010

Keywords:
A. Flexible composites
A. Layered structures
B. Delamination
B. Fracture
Permeation barriers

ABSTRACT

Organic–inorganic multilayer permeation barriers are emerging as a promising solution to the stringent barrier requirement of flexible electronics. Yet the mechanical failure of the multilayer permeation barriers could be fatal to their barrier performance. We study two co-evolving failure mechanisms of the multilayer permeation barriers under tension, namely, the cracking of the inorganic oxide layer and the delamination along the oxide–organic interface, using computational modeling. An effective driving force for the oxide layer cracking is determined, which decreases as the oxide–organic interfacial adhesion increases. Emerging from the study is a simple but effective design to enhance the deformability of multilayer permeation barriers by applying a thin protective coating. Further studies show that strong adhesion of the coating-oxide interface is crucial for the coating performance. The results from this study provide quantitative guidance for the material selection and structural optimization of organic–inorganic multilayer permeation barriers of high mechanical durability.

© 2010 Elsevier Ltd. All rights reserved.

1. Introduction

The past decade has seen a wealth of research on flexible electronics, an emerging technology with an array of promising applications, such as paper-like displays and organic light emitting diodes (OLEDs) [1–5]. Flexible electronics are attractive for their large deformability, low weight, large surface areas, and low cost. Organic materials (e.g., polymers) make these attributes possible. For example, the emissive electroluminescent layer of OLEDs is composed of a thin film of organic compounds; and flexible devices are often fabricated on thin polymer substrates. The functional organic materials used in flexible devices are extremely vulnerable to moisture [6–10], thus result in a rather limited device lifetime—a grand challenge to the future success of flexible electronics technology. A natural choice for long-lasting flexible devices is to protect them with permeation barriers. Organic–inorganic multilayer permeation barriers are emerging as a promising solution to the stringent barrier requirement of flexible electronics [11–13]. The mechanical failure of the multilayer permeation barriers under large deformation, however, could be fatal to the barrier performance [13]. So far, little attention, if any [14,15], has been given to the failure mechanics of multilayer organic–inorganic permeation barriers. To address this largely unexplored issue, in this paper we study two co-evolving tensile failure mechanisms of the multilayer permeation barriers, namely, channel cracking and interfacial delamination, through systematic computational modeling. Emerging from our study is a simple but effective design to enhance the durability of multilayer permeation barriers by applying a thin protective coating.

Designing a permeation barrier to allow a reasonable service life of flexible devices is remarkably challenging, with a design criteria over three orders of magnitude more stringent than that of traditional barriers in terms of water vapor permeation rate [13,16]. Furthermore, the large and repeated deformation that flexible devices undergo also requires that the permeation barriers be rugged. Organic materials (e.g., polymers) are often rugged but highly permeable to moisture, while inorganic materials (e.g., ceramics and glass) are almost impermeable to moisture but extremely fragile. Thus, neither by itself is an effective permeation barrier for flexible electronics. Such a conundrum has led to the design of multilayer barrier coatings consisting of alternating thin films of inorganic and organic materials, with the hope to capitalize on both the impermeability of the inorganic layers and the ruggedness of the organic layers [15,18,19]. For example, a multilayer barrier made of a stack of alternating layers of polyacrylate and Al_2O_3 (e.g., Fig. 1a) has been demonstrated to meet the stringent design criteria at ambient conditions [11,12]. Such a promising barrier performance, however, was achieved in the as-made barriers that are not subject to large mechanical deformation.

---

[*] Corresponding author at: Department of Mechanical Engineering, University of Maryland, College Park, MD 20742, United States. Tel.: +1 301 405 0364; fax: +1 301 314 9477.
E-mail address: lit@umd.edu (T. Li).

0266-3538/$ - see front matter © 2010 Elsevier Ltd. All rights reserved.
doi:10.1016/j.compscitech.2010.12.003

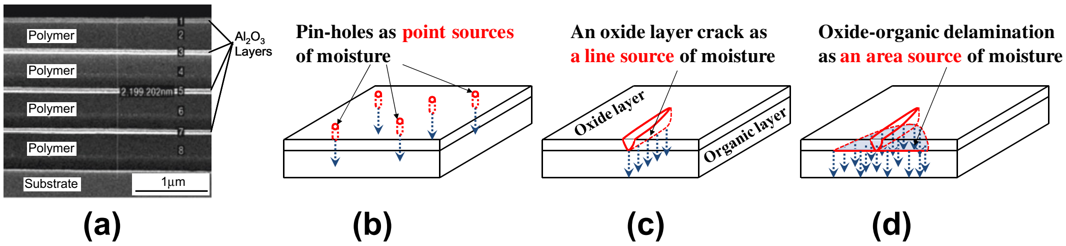
Polymer
Polymer
Polymer
Polymer
Substrate
1μm
Al_2O_3 Layers
Pin-holes as point sources of moisture
An oxide layer crack as a line source of moisture
Oxide layer
Organic layer
Oxide-organic delamination as an area source of moisture
(a)
(b)
(c)
(d)

Fig. 1. (a) Scanning electron microscope image of the cross section of an organic–inorganic multilayer permeation barrier (Courtesy of Vitex Sys. Inc.). Moisture can permeate through various defects in a permeation barrier, such as (b) pin-holes in an as-made barrier, (c) a channel crack in the oxide layer of a barrier, and (d) delamination along the oxide–organic interface in a barrier.

Given the stringent barrier requirements for flexible electronics, any mechanical failure in the brittle oxide films of the multilayer barriers would be fatal for barrier performance. While the organic layers in multilayer barriers are compliant and can recover from large strains, the oxide layers are brittle and fracture at small strains. Typical fracture modes include channel cracks in the oxide layers and delamination along the oxide–organic interfaces. Moisture permeates through an as-made multilayer barrier mainly via the pin-hole defects in the oxide layers (Fig. 1b) [17,20]. By contrast, a channel crack in the oxide layer can substantially increase moisture permeation through the barrier by opening *a line source of moisture* (Fig. 1c), rather than the point source from the initial pin-holes. The situation becomes even worse when oxide–organic interfacial delamination accompanies the channel crack propagation, because the moisture wicking along the delaminated interface results in *an area source of moisture* at the delamination site, as illustrated in Fig. 1d. Therefore, fracture-induced defects (i.e., channel cracks and interfacial delamination) are expected to drastically accelerate moisture permeation through the barrier, and hence are fatal to the flexible devices. As a result, to study the barrier performance under large mechanical deformation, it is imperative to investigate the failure mechanism of the organic–inorganic hybrid layered structures.

Fracture mechanics of thin brittle films on rigid substrates has been a focal topic in the discipline of solid mechanics in the past two decades. Existing studies have largely originated from the context of traditional microelectronics [21–28], thus focused on film-substrate structures with comparable stiffness and subject to small strains (~1%). For flexible devices, the large difference in stiffness of the constituent materials of permeation barriers (e.g., the Young's modulus of Al_2O_3 is more than 100 times higher than that of polyacrylate) and the large mechanical deformation they undergo leads to rich but complicate failure behaviors that have not yet been clearly described in existing studies. On the research front of the fracture of thin brittle films on compliant substrates, Cotterell and Chen [29] investigated the buckling and cracking of thin films on compliant substrate under compression; Ambrico and Begley [30] explored the role of substrate compliance on steady-state channel cracking in a brittle film. Mei et al. [31] investigated the effect of interfacial delamination on channel cracking of a brittle thin film on an elastic substrate. These studies mainly focused on the fracture of film-on-substrate *bi-layer* structures, which shed important lights on but cannot fully capture the fracture characteristics of the *multilayer* organic–inorganic permeation barriers. For example, the channel cracking of an oxide layer and the interfacial delamination in a multilayer permeation barrier can be constrained by the presence of adjacent stiff oxide films. Such a constraint is, in turn, mediated by the thickness of the compliant organic layer in between two oxide films. Therefore, it is expected that the failure mechanics of a multilayer permeation barrier made of alternating organic–inorganic stack is different from that of a film-on-substrate bi-layer. Cordero et al. [14] studied the critical strains for various configurations of channel cracks in an inorganic–organic–inorganic tri-layer permeation barrier on a polymer substrate. In that study, however, the organic–inorganic interfaces were assumed to remain perfectly bonded as channel crack propagates, thus no interfacial delamination was considered.

When a multilayer permeation barrier is under large deformation, it is highly possible that the oxide–organic interfacial delamination and the channel cracking of the oxide layer facilitate each other and thus co-evolve. On one hand, as the delaminated oxide layer becomes freestanding, it induces a larger driving force for channel crack propagation. On the other hand, the channel crack exerts more concentrated traction on the interface at the delamination front, promoting further delamination. The co-evolution of interfacial delamination and necking fracture of a thin Cu film on a compliant polyimide substrate under large tensile deformation has been predicted in computational modeling [32] and further observed in recent experiments [33,34].

Aiming to understand the yet unexplored mechanisms that govern the mechanical durability of organic–inorganic multilayer permeation barriers, we study the co-evolving channel cracking and interfacial delamination in such barriers under tension, through computational modeling. The rest of the paper is organized as follows. Section 2 describes the computational model; Section 3 reports the driving force for oxide–organic interfacial delamination in the applied tension direction, from which the effective driving force for steady state oxide layer channel cracking perpendicular to the applied tension direction can be obtained. Section 4 shows that a thin, compliant protective coating over the top oxide layer can effectively reduce the driving forces for both channel cracking and interfacial delamination. Section 5 discusses the role of the protective coating can be compromised if coating-oxide interfacial delamination occurs. The main research findings of this paper are summarized in Section 6.

2. Computational model

It has been shown that [14], if the organic layers are thicker than the oxide layers in a multilayer permeation barrier, channel cracking in the top oxide layer requires the least driving force when compared with other tensile failure modes (e.g., parallel channel cracking in multiple oxide layers, or channel cracking across the entire thickness of the coating). In the real design of multilayer permeation barriers (e.g., Fig. 1), the organic layers are often much thicker (e.g., 5–7 times) than the oxide layers. Therefore, it is reasonable to assume the dominant tensile failure mode of a real barrier to be the channel cracking in the top oxide layer with possible interfacial delamination originating from the channel root. Since other oxide layers except the top one remains intact in this dominant failure mode, and the oxide layers are more than 100 times stiffer than the organic layers, it is justified to assume that the constraint from other layers of the barrier to the channel cracking and interfacial delamination of the top oxide layer is mainly due to the oxide layer next to the top one, while the contribution from other layers below, be it oxide or organic, is negligible. Above said, we model a tri-layer barrier (two oxide layers sandwiching an organic layer) perfectly bonded to a thick polymer substrate, and analyze the tensile failure of this structure using the finite element code ABAQUS.

Fig. 2 illustrates the fracture of a blanket tri-layer barrier on a polymer substrate subject to uniaxial tension. Under sufficiently large tension, cracks initiate from built-in imperfections (e.g., pinholes, edges or corners) in the oxide layer and further propagate to form channel cracks. The stress concentration near the channel root can be severe enough to cause interfacial delamination. As to be shown in Section 3, under tension, the driving force for interfacial delamination decreases as the delamination advances in the tensile direction. As a result, the interfacial delamination eventually stops advancing in the tensile direction when such a driving force becomes smaller than the oxide–organic interfacial toughness. On the other hand, the channel crack continues propagating in the direction perpendicular to the applied tension and so does the concomitant interfacial delamination near the root of the channel crack front.

The detailed shape and deformation state near the front of the channel crack and the concomitant interfacial delamination can be rather complicated, and thus hard to predict. By contrast, far ahead and far behind the cracking and delamination front, the structure can be taken to deform under the plane strain conditions. To compute the driving force for interfacial delamination in the tensile direction, we simulate a slice of material of unit thickness far behind the cracking and delamination front and calculate the energy release rate at the delaminating front in the tensile direction using contour integral available in ABAQUS. Taking all materials in the structure to be linearly elastic, the driving force for both the channel cracking and the interfacial delamination to propagate in the direction perpendicular to the applied tension can be calculated by the elastic energy stored in a slice of material of unit thickness far ahead of the fracture front minus the elastic energy stored in a slice of material of unit thickness far behind the fracture front.

In the simulations, the two oxide layers are of thickness h, the organic layer between two oxide layers is of thickness H, and the polymer substrate is of thickness $1000h$ and length $1000h$. The horizontal displacement is set to be zero along the centerline of the laminate, and set to be u along both sides of the laminate. The quantity $\varepsilon = u/500h$ will be called the applied strain. Far behind the channel front, the width of the oxide–organic interfacial delamination originated from the channel root is d_{oo} at each side. In simulations, we fix the ratio $H/h = 5$ but vary the ratio d_{oo}/h to study its effect on the driving force for delamination. In the region near the tip of the interfacial delamination, both the oxide film and the organic layer are densely meshed into four-node quadrilateral plane strain concentric-circle elements. The portion outside of this region are meshed with triangle plane strain elements of matching sizes near the regions and coarser elements far away from the regions to reduce the computation time. In the simulations, the Young's modulus and the Poisson's ratio of the oxide layer are $E_{oxide} = 300$ GPa and $\nu_{oxide} = 0.3$, respectively, and those of the organic layer are $E_{organic} = 2$ GPa and $\nu_{organic} = 0.3$, respectively. The Young's modulus and the Poisson's ratio of the substrate are taken to be the same as that of the organic layer, respectively. These values are representative of an Al_2O_3-polyacrylate multilayer permeation barrier on a polyethylene terephthalate substrate.

3. Driving forces for interfacial delamination and channel cracking in a multilayer permeation barrier under tension

The driving force for interfacial delamination *in the tensile direction* far behind the channel front (e.g., inset of Fig. 3a) can be represented by the energy release rate at the delamination front. Dimensional considerations lead to this energy release rate taking the form

$$G_d = f\left(\frac{d_{oo}}{h}, \frac{E_{organic}}{E_{oxide}}, \frac{H}{h}\right) E^*_{oxide}\varepsilon^2 h, \qquad (1)$$

where $E^*_{oxide} = E_{oxide}/(1 - \nu^2_{oxide})$ is the plane strain modulus of the oxide. The dimensionless function f denotes the normalized driving force of interfacial delamination and can be calculated numerically by contour integral using finite element method.

Fig. 3a plots normalized driving force of interfacial delamination $G_d/E^*_{oxide}\varepsilon^2 h$ as a function of normalized delamination width d_{oo}/h. When the delamination width is small (e.g., $d_{oo}/h < 1$), the stress concentration near the channel crack root leads to a significantly large driving force of interfacial delamination. As the delamination width increases, the driving force of interfacial delamination drops considerably when $d_{oo}/h < 10$ and then gradually reaches a plateau when $d_{oo}/h > 10$. The initiation and propagation of the interfacial delamination is governed by the competition between driving force G_d and oxide–organic interfacial toughness Γ_{oo}. Fig. 3a indicates that, for a modest oxide–organic interfacial toughness, delamination can initiate at the channel crack root. As the delamination advances along the interface in the tensile direction, the driving force decreases. The delamination eventually

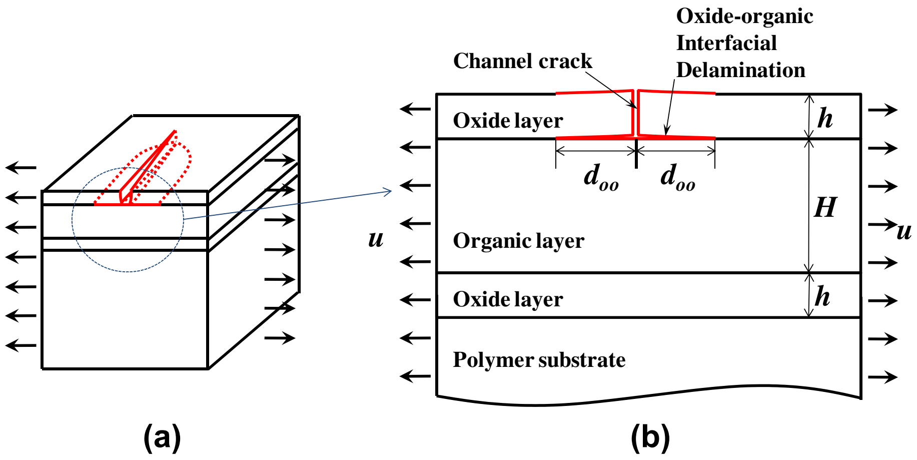

Fig. 2. Schematic of (a) the computational model considering (b) both the channel cracking of the oxide layer and the concomitant oxide–organic interfacial delamination.

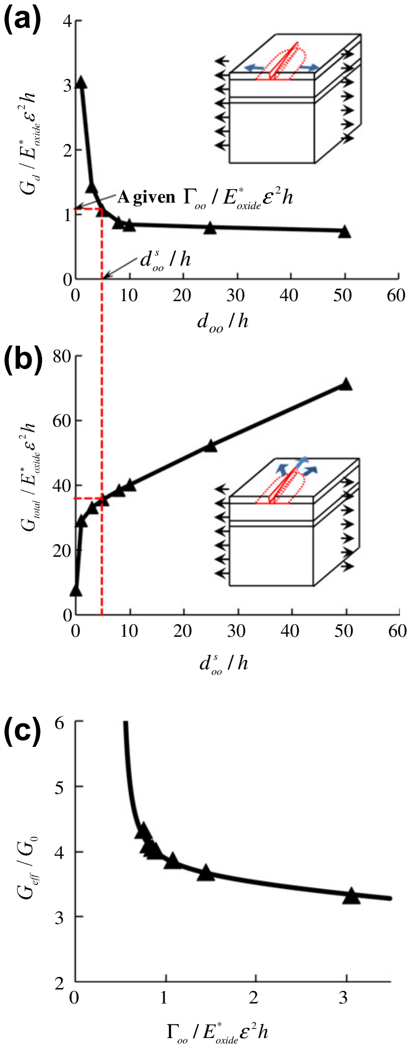

Fig. 3. (a) Normalized driving force of interfacial delamination along tensile direction $G_d/E^*_{oxide}\varepsilon^2 h$ as a function of normalized delamination width d_{oo}/h; (b) Normalized driving force of oxide cracking and interfacial delamination perpendicular to tensile direction $G_{total}/E^*_{oxide}\varepsilon^2 h$ as a function of normalized steady-state delamination width d^s_{oo}/h. Dash lines: for a given interfacial toughness Γ_{oo} the corresponding steady-state delamination width d^s_{oo} can be determined from (a), from which G_{total} can be further determined in (b). (c) Normalized effective driving force for channel cracking G_{eff}/G_0 as a function of normalized interfacial toughness $\Gamma_{oo}/E^*_{oxide}\varepsilon^2 h$. Here $G_0 = G_{total}(d^s_{oo} = 0)$.

stops propagating at a width, d^s_{oo}, where the driving force drops to the value of the interfacial toughness, i.e., $G_d = \Gamma_{oo}$.

We next compute the total driving force G_{total} for both the channel cracking and the interfacial delamination to propagate *in the direction perpendicular to the applied tension* (e.g., inset of Fig. 3b). G_{total} takes a form similar to Eq. (1) but with a different dimensionless function *f*. As discussed in Section 2, the stress state and deformation characteristics near the channel cracking front and the concomitant interfacial delamination are rather complicated. Assuming the structure deforms elastically, G_{total} can be calculated by comparing the elastic energy stored in a slice of material of unit thickness far ahead of the fracture front and that stored in a slice of material of unit thickness far behind the fracture front. We consider the steady-state fracture process where far behind the channel cracking front the oxide–organic interfacial delamination reaches a constant width of d^s_{oo}. Fig. 3b plots $G_{total}/E^*_{oxide}\varepsilon^2 h$ as a function of the normalized steady-state delamination width d^s_{oo}/h. In the case of perfect bonding between the oxide layer and the organic layer (e.g., no interfacial delamination, $d^s_{oo}/h = 0$), G_{total} corresponds to the driving force for pure channel cracking, which agrees with previous study [14,31]. Once interfacial delamination occurs and advances, G_{total} increase significantly. This can be explained by the considerable elastic energy released from the delaminated portion of the oxide layer in the wake of the channel cracking due to the loss of substrate constraint. For example, compared with the case without interfacial delamination, G_{total} triples for $d^s_{oo}/h = 1$ and increases nearly sixfold for $d^s_{oo}/h = 25$. By contrast, if there is no interfacial delamination, only a narrow region in the oxide layer along the channel crack surface can be relaxed, leading to a modest elastic energy release. The condition for steady-state channel cracking and interfacial delamination can be described as

$$G_{total} \geqslant \Gamma_{oxide} + 2\Gamma_{oo} d^s_{oo}/h, \tag{2}$$

where Γ_{oxide} is the cohesive fracture toughness of the oxide layer, and the second term on the right denotes the energy required for the oxide–organic interfacial delamination accompanying per unit area advance of the channel crack.

For a given oxide–organic interfacial toughness Γ_{oo}, one can determine the corresponding steady-state delamination width d^s_{oo} (e.g., Fig. 3a), from which one can further obtain G_{total} (e.g., Fig. 3b). In this sense, both d^s_{oo} and G_{total} are functions of Γ_{oo}. By moving the term of $2\Gamma_{oo} d^s_{oo}/h$ in Eq. (2) to the left-hand side, an effective driving force for steady-state channel cracking of the oxide layer can be defined as

$$G_{eff} = G_{total} - 2\Gamma_{oo} d^s_{oo}/h, \tag{3}$$

and thus the condition for steady-state channel cracking can be given by

$$G_{eff} \geqslant \Gamma_{oxide}, \tag{4}$$

in which the right-hand side denotes the resistance that is independent of the interfacial property, and the left-hand side represents the driving force that is a function of the oxide–organic interfacial toughness.

Fig. 3c plots the normalized effective driving force for channel cracking G_{eff}/G_0 as a function of normalized interfacial toughness $\Gamma_{oo}/E^*_{oxide}\varepsilon^2 h$. Here G_0 is the driving force for channel cracking without oxide–organic interfacial delamination, i.e., $G_0 = G_{total}(d^s_{oo} = 0)$ as in Fig. 3b. The smaller the oxide–organic interfacial toughness, the larger the steady-state delamination width, and therefore, the larger the effective driving force for channel cracking of the oxide layer.

4. Effect of a protective coating on the durability of a multilayer permeation barrier

The results in Section 3 show that the tensile failure of the organic–inorganic multilayer permeation barriers is driven by the elastic energy release due to the channel cracking of the top oxide layer and the delamination along the oxide–organic interface. To enhance the mechanical durability of the multilayer permeation barriers under tension, we propose to add a thin deformable protective coating (e.g., a polymeric material) onto the surface of the top oxide layer in the permeation barrier. The polymeric coating can sustain large tensile deformation without rupture, therefore can offer additional mechanical constraint that leads to a reduced driving force for the channel cracking and interfacial delamination in the permeation barriers. In this section, we quantify the reduction of these driving forces as a function of the stiffness and thickness of the protective coating. Here we assume a perfect bonding between the protective coating and the top oxide layer, i.e., no coating-oxide delamination. The effect of possible delamination along the coating-oxide interface will be discussed in Section 5.

4.1. Reduced driving force for oxide layer cracking without oxide–organic delamination

When a multilayer permeation barrier with a thin protective coating is under tension, the cracks may initiate from pre-existing imperfections in top oxide layer and then tunnel through. Due to the mechanical constraint of the protective coating, the elastic energy released by such a tunnel crack is less than that by a channel crack in a bare permeation barrier without protective coating.

Fig. 4 plots the normalized driving force $G_0^p/E^*_{oxide}\varepsilon^2 h$ for a tunnel crack in the top oxide layer of a permeation barrier with a protective coating of thickness h_p, as a function of the stiffness of the protective coating E_p. Here we assume that no oxide–organic interfacial delamination occurs. For comparison, the driving force for a channel crack in the top oxide layer of a bare permeation barrier without oxide–organic interfacial delamination $G_0/E^*_{oxide}\varepsilon^2 h$ is also included (the dash line). There is a nearly fourfold decrease in the driving force of oxide layer cracking when a protective coating is applied. Such a drastic decrease in fracture driving force also shows weak dependence on the stiffness and thickness of the protective coating. For example, a very compliant protective coating (e.g., E_p = 2 MPa) of the same thickness of the oxide layer can lead to a similar reduction of crack driving force comparable to that due to a stiff and thick protective coating (e.g., with a stiffness of 20 GPa and a thickness ten times of the oxide layer).

4.2. Reduced driving force for oxide layer cracking with oxide–organic delamination

We now consider the case where delamination along the oxide–organic interface can emanate from the root of a tunnel crack in the top oxide layer of a permeation barrier with protective coating. In such a case, the protective coating is expected to constrain the opening of the tunnel crack, thus leading to a limited relaxation of the elastic energy in the debonded portion of the oxide layer and organic layer, therefore resulting in a decrease in the driving forces for both interfacial delamination and tunnel cracking.

The driving force for the oxide–organic interfacial delamination in the tensile direction far behind the channel front now takes the form

$$G_d^p = f_p\left(\frac{d_{oo}}{h}, \frac{E_{organic}}{E_{oxide}}, \frac{E_p}{E_{oxide}}, \frac{H}{h}, \frac{h_p}{h}\right)E^*_{oxide}\varepsilon^2 h. \tag{5}$$

Fig. 5a plots the normalized driving force for interfacial delamination $G_d^p/E^*_{oxide}\varepsilon^2 h$ as a function of the steady-state delamination width d^s_{oo}/h, for various stiffness of the protective coating (i.e., E_p = 2 MPa, 20 MPa, 200 MPa, 2 GPa and 20 GPa, which are representative of polymers ranging from very compliant elastomers to stiff plastics). Here the thickness of the protective coating is taken to be the same as that of the oxide layer, i.e., $h_p/h = 1$. When compared with the case of no protective coating (i.e., Fig. 3a), Fig. 7a clearly shows that, a thin ($h_p/h = 1$) and compliant (e.g., E_p = 2 MPa) protective coating can significantly reduce the driving force for the oxide–organic interfacial delamination. For example, when $d^s_{oo}/h \leqslant 10$, the reduction of the delamination driving force is approximately threefold if a protective layer is applied. When $d^s_{oo}/h \geqslant 25$ the protective layer reduces the delamination driving force to nearly zero. Furthermore, this reduction of the delamination driving force remains nearly independent of the protective coating stiffness, unless a very stiff polymer coating (e.g., E_p = 20 GPa) is applied, which leads to an even more substantial reduction of the delamination driving force.

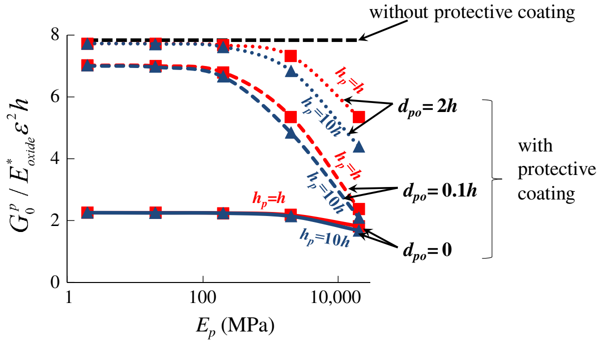

Fig. 4. Solid lines with markers plot normalized driving force $G_0^p/E^*_{oxide}\varepsilon^2 h$ for a tunnel crack in the top oxide layer of a permeation barrier with a protective coating of thickness h_p, as a function of the stiffness of the protective coating E_p. Here there is no coating-oxide interfacial delamination, (i.e., $d_{po}/h = 0$). The horizontal dash line denotes $G_0/E^*_{oxide}\varepsilon^2 h$, the normalized driving force for a channel crack in the top oxide layer of a bare permeation barrier. The curved dash and dotted lines with markers plot normalized driving force for oxide layer cracking as a function of E_p, for h_p/h = 1 and 10, and d_{po}/h = 0.1 and 2, respectively.

When a protective coating is applied, the total driving force G^p_{total} for both the tunnel cracking and the interfacial delamination to propagate in the direction perpendicular to the applied tension takes a form similar to Eq. (5) but with a different dimensionless function f_p. Using the similar modeling strategy in Section 3, G^p_{total} can be computed and is plotted as a function of the normalized steady-state delamination width d^s_{oo}/h, as shown in Fig. 5b. Here, $h_p/h = 1$. When compared with the case of no protective coating (i.e., Fig. 3b), Fig. 5b also clearly shows substantial reduction of the total driving force G^p_{total}. For example, when $d^s_{oo}/h \leq 10$, the reduction of G^p_{total} is more than fourfold if a protective coating is applied. When $d^s_{oo}/h \geqslant 25 G^p_{total}/E^*_{oxide}\varepsilon^2 h$ reaches a plateau of about 12.8. By contrast, if there is no protective coating (e.g., Fig. 3b), the total driving force increases approximately linearly with d_{oo}/h when $d^s_{oo}/h \geqslant 25$. Fig. 5b also shows a dependence of the reduction of G^p_{total} on the stiffness of the protective coating similar to that in Fig. 7a. Fig. 5c and d further plot $G_d^p/E^*_{oxide}\varepsilon^2 h$ as a function of d^s_{oo}/h and $G^p_{total}/E^*_{oxide}\varepsilon^2 h$ as a function of d^s_{oo}/h for the case of $h_p/h = 10$, respectively. A thicker protective coating can result in more substantial reduction of $G_d^p/E^*_{oxide}\varepsilon^2 h$ and $G^p_{total}/E^*_{oxide}\varepsilon^2 h$. The dependence of the reduction of fracture driving force on protective coating stiffness is also stronger when a thicker protective coating is applied.

Following the similar procedure in Section 3, an effective driving force for steady-state tunnel cracking of the oxide layer can be defined as

$$G^p_{eff} = G^p_{total} - 2\Gamma_{oo} d^s_{oo}/h, \tag{6}$$

which takes into account of the effects of both the oxide–organic delamination and that of the protective coating. Fig. 6 plots $G^p_{eff}/E^*_{oxide}\varepsilon^2 h$ as a function of normalized interfacial toughness $\Gamma_{oo}/E^*_{oxide}\varepsilon^2 h$. Here $h_p/h = 1$. Fig. 6 clearly shows that, for a given oxide–organic interfacial toughness, the effective driving force for oxide layer cracking can be considerably reduced when a thin and compliant protective coating is applied on the top of the oxide layer. Such a reduction of effective driving force for oxide layer cracking is nearly independent of stiffness of the protective coating when $E_p \leqslant 2$ GPa. A very stiff plastic protective coating (e.g., E_p = 20 GPa) can further reduce the effective cracking driving force modestly.

The results in this section reveal a simple but effective design strategy to improve the durability of the organic–inorganic multilayer permeation barriers in flexible electronics. Well bonded to the surface of the top oxide layer, even a thin and compliant protective coating (e.g., an elastomeric layer with a thickness comparable to that of the oxide layer) can considerably reduce the driving forces for the tunnel cracking of the top oxide layer and the oxide–organic interfacial delamination. In other words, a multilayer permeation

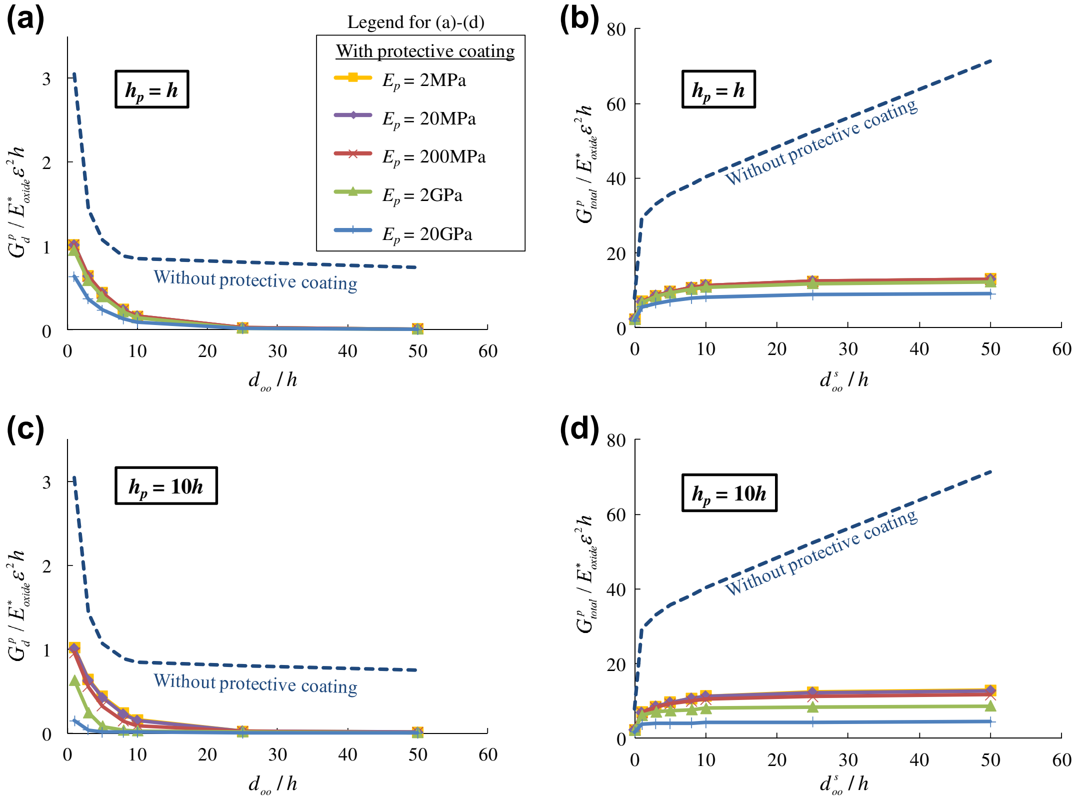

Fig. 5. (a) $G_d^p/E^*_{oxide}\varepsilon^2 h$ as a function of d_{oo}/h. Here $h_p/h = 1$; (b) $G^p_{total}/E^*_{oxide}\varepsilon^2 h$ as a function of d^s_{oo}/h. Here $h_p/h = 1$; (c) $G_d^p/E^*_{oxide}\varepsilon^2 h$ as a function of d_{oo}/h. Here $h_p/h = 10$; (d) $G^p_{total}/E^*_{oxide}\varepsilon^2 h$ as a function of d^s_{oo}/h. Here $h_p/h = 10$. Various stiffness of the protective coating are used.

barrier with a protective coating can sustain larger elongations before fracture than a bare multilayer permeation barrier.

5. Discussion

The reduction of the fracture driving forces reported in Section 4 results from the constraint of the protective coating to the elastic energy release in the wake of oxide layer tunnel cracking and oxide–organic interfacial delamination. If the adhesion between the protective coating and the top oxide layer is not sufficiently strong, the stress concentration due to the tunnel cracking near the coating-oxide interface may cause delamination. As a result, the mechanical constraint of the protective coating to the top oxide layer is weakened, leading to a less substantial reduction of the driving force for oxide layer tunnel cracking and oxide–organic interfacial delamination.

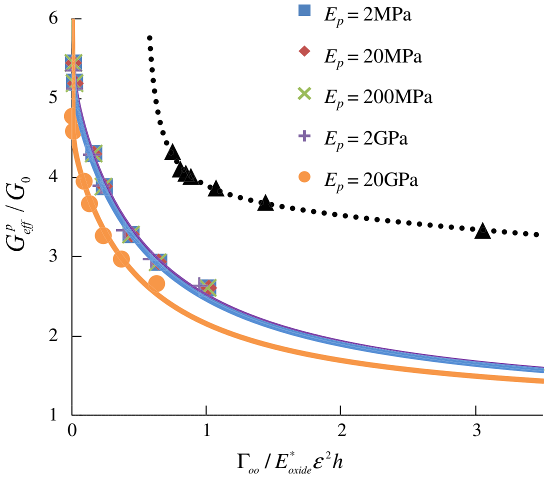

Fig. 6. $G^p_{eff}/E^*_{oxide}\varepsilon^2 h$ as a function of normalized interfacial toughness $\Gamma_{oo}/E^*_{oxide}\varepsilon^2 h$ for various stiffness of the protective coating. Here $h_p/h = 1$.

To study the impact of possible delamination along the interface between the protective coating and the top oxide layer, we simulate two cases: (1) delamination occurs only along the coating-oxide interface; (2) delaminations occur along both the coating-oxide interface and the oxide–organic interface.

The simulation results for case 1 are presented in Fig. 4 (dash and dotted lines with markers), which plots the normalized driving force for oxide layer cracking as a function of the protective coating stiffness E_p, for two protective coating thickness, $h_p/h = 1$ and 10, and two coating-oxide delamination length, $d_{po}/h = 0.1$ and 2, respectively. If the protective coating is stiff and relatively thick (e.g., $E_p = 20$ GPa and $h_p/h = 10$), the reduction of the driving force for oxide layer cracking decreases from nearly fourfold to nearly twofold, if a delamination of length $d_{po} = 2h$ occurs along the coating-oxide interface. If the protective coating is too compliant (e.g., $E_p = 20$ MPa), a small delamination (e.g., $d_{po}/h = 0.1$) along the coating-oxide interface can lead to a driving force for oxide layer cracking comparable to that in a permeation barrier without protective coating.

The simulation results for case 2 are presented in Fig. 7, and compared with the results in Fig. 5a and b. In case 2, a delamination of length $d_{po} = h$ along the coating-oxide interface is prescribed. In comparison with Figs. 5a and 7a plots the normalized driving force for oxide–organic interfacial delamination in the tensile direction as a function of d^s_{oo}/h. For a compliant protective coating (e.g., $E_p \leqslant 200$ MPa), a short delamination along the coating-oxide interface results in an elevated driving force for oxide–organic interfacial delamination comparable to that of a

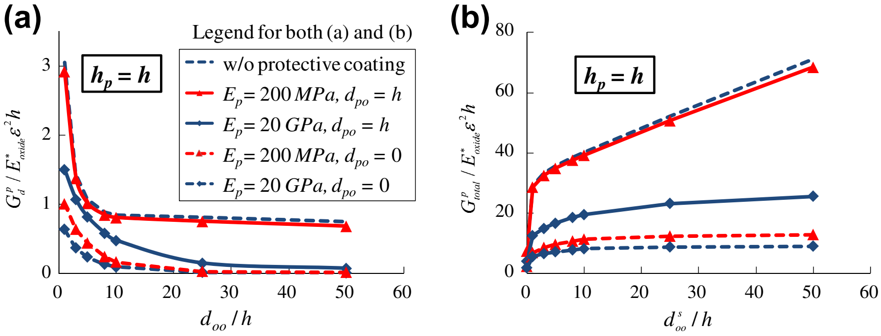

Fig. 7. Impact of the coating-oxide interfacial delamination on (a) the driving force for oxide–organic interfacial delamination along the tensile direction and on (b) the driving force for both oxide layer cracking and oxide–organic interfacial delamination perpendicular to the tensile directions. Here $h_p/h = 1$. The corresponding curves in Fig. 5 are included for comparison (dash line and dash lines with markers).

bare permeation barrier. In other words, a compliant protective coating debonded from the oxide layer can only provide negligible mechanical constraint to the elastic energy release in the wake of oxide tunnel cracking. For a stiff protective coating (e.g., $E_p = 20$ GPa), a short delamination along the coating-oxide interface leads to a modest increase in the driving force for oxide–organic interfacial delamination when d_{oo}^s/h is small. Such an increase gradually diminishes when $d_{oo}^s/h \geqslant 25$. In comparison with Fig. 5b, Fig. 7b plots the normalized total driving force for both the tunnel cracking and the interfacial delamination to propagate in the direction perpendicular to the applied tension as a function of d_{oo}^s/h. A short delamination along the coating-oxide interface induces a loss of mechanical constraint of a compliant protective coating similar to that shown in Fig. 7a. When a stiff protective coating is applied, the loss of mechanical constraint is partial and remains to be approximately constant as d_{oo}^s/h increases.

The above simulation results show that, delamination along the coating-oxide interface is detrimental for a compliant protective coating, causing nearly the loss of its mechanical constraint. On the other hand, a stiff protective coating can tolerate short delamination along the coating-oxide interface by providing partial mechanical constraint to the failure of the permeation barrier. The results in Figs. 4 and 7 can offer quantitative guidelines for the material selection and interface adhesion control of the protective coating.

6. Concluding remarks

We study the tensile failure of organic–inorganic multilayer permeation barriers in flexible electronics. Major findings of the present study are recapped as follows:

1. Two failure mechanisms that are fatal for the barrier performance, namely, oxide layer cracking and oxide–organic interfacial delamination, facilitate each other, and thus co-evolve.
2. The driving force for the oxide–organic delamination along the tensile direction and that for the oxide layer cracking and the concomitant oxide–organic delamination perpendicular to the tensile direction are quantitatively determined, from which an effective driving force for the oxide layer cracking is defined and shown to decrease as the oxide–organic interfacial adhesion increases. This suggests that a strong interlayer adhesion is crucial for the mechanical durability of the multilayer hybrid permeation barriers.
3. A structural design strategy to enhance the mechanical durability of the multilayer permeation barriers emerges from the study. We show that a thin, compliant and well bonded protective coating can offer effective mechanical constraint to the permeation deformation and thus substantially decrease the effective driving force for oxide cracking by several folds.
4. Further studies show that strong adhesion between the protective coating and the top oxide layer is crucial for the coating performance. Delamination along the coating-oxide interface can result in partial or nearly total loss of the mechanical constraint from the protective coating, depending on the stiffness of the coating.

The results from the present study are expected to offer mechanistic understanding of the failure mechanics of organic–inorganic multilayer permeation barriers in flexible electronics. The simple but effective strategy of applying a protective coating can potentially improve the mechanical durability of the permeation barriers. While the results from this study can provide quantitative guidance for the material selection and structural optimization of the permeation barriers, further experimental investigation are needed to validate the research findings in this paper.

Acknowledgments

This research is supported by National Science Foundation (under Grants 0856540 and 0928278) and Minta Martin Foundation.

References

[1] Forrest S. The path to ubiquitous and low-cost organic electronic appliances on plastic. Nature 2004;428:911–8.
[2] Reuss RH et al. Macroelectronics: perspectives on technology and applications. Proc IEEE 2005;93:1239–56.
[3] Nathan A, Chalamala BR. Flexible electronics technology, part II: materials and devices. Proc IEEE 2005;93:1391–3.
[4] Crawford GP. Flexible flat panel displays. Chichester; Hoboken (NJ): John Wiley&Sons; 2005.
[5] Rogers JA, Someya T, Huang YG. Materials and mechanics for stretchable electronics. Science 2010;327:1603–7.
[6] McElvain J, Antoniadis H, Hueschen MR, Miller JN, Roitman DM, Sheats JR, et al. Formation and growth of black spots in organic light-emitting diodes. J Appl Phys 1996;80:6002–7.
[7] Sutherland DGJ et al. Photo-oxidation of electroluminescent polymers studied by core-level photoabsorption spectroscopy. Appl Phys Lett 1996;68:2046–8.
[8] Liew YF, Aziz H, Hu NX, Chan HSO, Xu G, Popovic Z. Investigation of the sites of dark spots in organic light-emitting devices. Appl Phys Lett 2000;77:2650–2.
[9] Papadimitrakopoulos F, Zhang XM, Higginson KA. Chemical and morphological stability of aluminum tris(8-hydroxyquinoline) (Alq(3)): effects in light-emitting devices. IEEE J Selected Topics Quant Electron 1998;4:49–57.
[10] Schaer M, Nuesch F, Berner D, Leo W, Zuppiroli L. Water vapor and oxygen degradation mechanisms in organic light emitting diodes. Adv Funct Mater 2001;11:116–21.
[11] Nisato G, Kuilder M, Bouten P, Moro P, Philips LO, Rutherford N. Thin film encapsulation for OLEDs: evaluation of multilayer barriers using the Ca test. SID Int Symp Digest Tech Papers 2003:550–3.
[12] Moro L, Krajewski TA, Rutherford N, Philips O, Visser RJ, Gross M, et al. Integrated encapsulation of bottom and top emission OLED displays. SPIE-The Int. Soc. Optic. Eng., Organic Light-Emitting Materials and Devices VIII; 2004.
[13] Lewis JS, Weaver MS. Thin-film permeation-barrier technology for flexible organic light-emitting devices. Selected Topics Quant Electron IEEE J 2004;10:45–57.
[14] Cordero N, Yoon J, Suo ZG. Channel cracks in a hermetic coating consisting of organic and inorganic layers. Appl Phys Lett 2007;90:111910.

[15] Chwang AB, Rothman MA, Mao SY, Hewitt RH, Weaver MS, Silvernail JA, et al. Thin film encapsulated flexible organic electroluminescent displays. Appl Phys Lett 2003;83:413–5.

[16] Erlat AGn, Yan M, R. Duggal A. Substrates and thin-film barrier technology for flexible electronics; 2009. p. 413–49.

[17] Burrows PE, Graff GL, Gross ME, Martin PM, Hall M, Mast E, et al. Gas permeation and lifetime tests on polymer-based barrier coatings. Proc SPIE 2001:75.

[18] Weaver MS, Michalski LA, Rajan K, Rothman MA, Silvernail JA, Brown JJ, et al. Organic light-emitting devices with extended operating lifetimes on plastic substrates. Appl Phys Lett 2002;81:2929–31.

[19] Kim TW, Yan M, Erlat G, McConnelee PA, Pellow M, Deluca J, et al. Transparent hybrid inorganic/organic barrier coatings for plastic organic light-emitting diode substrates. J Vac Sci Techol A 2005;23:971–7.

[20] Graff GL, Williford RE, Burrows PE. Mechanisms of vapor permeation through multilayer barrier films: lag time versus equilibrium permeation. J Appl Phys 2004;96:1840–9.

[21] Beuth JL. Cracking of thin bonded films in residual tension. Int J Solids Struct 1992;29:1657–75.

[22] Hutchinson JW, Suo Z. Mixed-mode cracking in layered materials. Adv Appl Mech 1992;29:63–191.

[23] Huang R, Prevost JH, Huang ZY, Suo Z. Channel-cracking of thin films with the extended finite element method. Eng Fract Mech 2003;70:2513–26.

[24] Vlassak JJ. Channel cracking in thin films on substrates of finite thickness. Int J Fract 2003;119:299–323.

[25] Tsui TY, McKerrow AJ, Vlassak JJ. Constraint effects on thin film channel cracking behavior. J Mater Res 2005;20:2266–73.

[26] Ma Q. A four-point bending technique for studying subcritical crack growth in thin films and at interfaces. J Mater Res 1997;12:840–5.

[27] Ho S, Suo Z. Tunneling cracks in constrained layers. J Appl Mech – Trans ASME 1993;60:890–4.

[28] Liu XH, Lane MW, Shaw TM, Simonyi E. Delamination in patterned films. Int J Solids Struct 2007;44:1706–18.

[29] Cotterell B, Chen Z. Buckling and cracking of thin films on compliant substrates under compression. Int J Fract 2000;104:169–79.

[30] Ambrico JM, Begley MR. The role of initial flaw size, elastic compliance and plasticity in channel cracking of thin films. Thin Solid Films 2002;419:144–53.

[31] Mei HX, Pang YY, Huang R. Influence of interfacial delamination on channel cracking of elastic thin films. Int J Fract 2007;148:331–42.

[32] Li T, Suo Z. Ductility of thin metal films on polymer substrates modulated by interfacial adhesion. Int J Solids Struct 2007;44:1696–705.

[33] Lu NS, Wang X, Suo ZG, Vlassak J. Metal films on polymer substrates stretched beyond 50%. Appl Phys Lett 2007;91:221909.

[34] Lu NS, Wang X, Suo Z, Vlassak J. Failure by simultaneous grain growth, strain localization, and interface debonding in metal films on polymer substrates. J Mater Res 2009;24:379–85.